



3D Finite Element Modelling of Weld Bead Penetration in Tungsten Inert Gas (TIG) Welding of AISI 1020 Low Carbon Steel Plate

Ikechukwu Owunna ^{1a}, Aniekan E. Ikpe ^{1b*} and J. I. Achebo ^{2a}

^{1ab}Department of Mechanical Engineering, University of Benin, P.M.B. 1154, Nigeria

^{2a}Department of Production Engineering, University of Benin, P.M.B. 1154, Nigeria

ORCID: A.Ikpe(0000-0001-9069-9676)

Abstract

Bead penetration depth plays a significant role on the quality and integrity of welds, as deeper penetration can improve the strength and load bearing capacity of weldments in service condition. Based on Design of Experiment (DOE), an experimental design matrix having thirteen (13) center points, six (6) axial points and eight (8) factorial points resulting in twenty (20) experimental runs was generated for TIG welding current, voltage, gas flow rate (L/min) and temperature. Maximum bead penetration of 8.44 mm was obtained from the FEM simulation with corresponding input variables of 190 A, 19 V, 18 L/min and 298.44 °C compared to maximum bead penetration of 7.942 mm obtained from the welding experimentation with corresponding input variables of 155 A, 22 V, 15.50 L/min and 278.46 °C. To clearly understand the rate of heat distribution across the as-welded plate, FEM bead penetration profiles were developed using Solid Works (2017 version) thermal transient analysis which revealed that the higher the temperature distribution the wider the Heat Affected Zones (HAZs) which are indications of phase transformations and alterations in mechanical properties of the welded metal which may lead to induced residual stresses if the welding parameters particularly the amperage is not controlled adequately. In addition, there was proximity in the trend of bead penetration from the regression plot where the FEM model had a coefficient of determination (R^2) of 0.9799 while R^2 of 0.9694 was obtained for the welding experimentation, indicating about 97.4% variance which in this context signifies that both bead penetration values can be adopted for real practical scenarios where deep weld bead penetrations are required.

Keywords: TIG welding, Bead penetration, Temperature, Heat distribution, Low carbon steel.

1. INTRODUCTION

Carbon steels have a wide range of application relevant to some industries such as marine industry, construction and automotive industry, chemical and petroleum industry etc. However, increased carbon content (typically at least 0.45% by weight) in the carbon steel implies increased hardness, increased tensile strength and difficulty in welding [1]. It is vital to achieve high quality welds which may depend on the type of welding, welding parameters, mechanical properties of welded metal, all of which contributes significantly to the strength behaviour of the welded metal in service condition [2]. Tungsten inert gas (TIG) welding is an arc welding process used in the fusion of two or more metals through the application of heat generated due to arc struck between a non-consumable tungsten electrode and the workpiece [3]. According to Memduh et al. [4], weld geometry parameters

consist of bead width, height of reinforcement, depth of penetration, wetting angle, electrode deposit area and plate fusion area. Weld bead penetration is the maximum distance between the surface of the base plate and depth to which the fusion has taken place in a weldment. In other words, it is the rate at which the fusion line extends below the surface of the welded material [5]. Weld penetration has a direct relationship with welding current, as increase or decrease in current can result in further increase or decrease in the weld penetration depth. Studies have shown that weld penetration is influenced by welding current, polarity, arc travel speed, electrode diameter etc. [6, 7]. Sushant [8] investigated the factors affecting bead penetration and observed that higher welding current provides deep penetration and lower current provides lower penetration depth. Effects of welding speed and heat input rate parameters on depth of penetration was investigated by Abbasi et al. [9] and the result reve-

*Corresponding author
Email: aniekan.ikpe@eng.uniben.edu



aled that bead depth increases with increase in heat input. Memduh et al. [10] noted that weld penetration is directly proportional to welding current, and that deep penetration can be achieved in operations where Direct Current Electrode Positive (DCEP) polarity is employed whereas, shallow penetration can be achieved as a result of Direct Current Electrode Negative (DCEN) polarity. Penetration decreases with the increase in welding speed because the time at which the arc force is allowed to penetrate into the material's surface decreases. Bead penetration decreases with increase in electrode diameter due to decrease in current density while high welding voltage produces wider and deeply penetrating welds than low welding voltages. Depth of penetration is maximum at optimum arc voltage [10]. Yadav et al. [11] observed that increase in welding voltage contributes to the increase in weld bead penetration. Tewari et al. [12] studied the effect of welding current, arc voltage, welding speed and heat input rate on the weldability of Mild Steel specimens of 50mm×40 mm×6 mm dimensions using metal arc welding. The result obtained showed that the depth of penetration increased with increasing welding speed up to 110.39 mm/min which was optimum value to obtain maximum penetration. However, increasing the speed of travel and maintaining constant arc voltage and current resulted in increased penetration until optimum speed was reached at which penetration was maximum, consequently, increasing the speed beyond the optimum rate resulted in decreased penetration. Ghazvinloo et al. [13] reported that if the welding speed decreases beyond a certain point, the penetration also will decrease due to the pressure of the large amount of weld pool beneath the electrode, which will cushion the arc penetrating force. Sudhakaran et al. [14] in their investigation noted that GTAW quality is mainly characterized by bead penetration depth. This is because shallow bead penetration is an influencing factor to the failure of a welded structure since penetration relates to the stress carrying capacity of a welded joint. Hence, the scope of this study is focused on investigating the interplay between TIG welding input process parameters (current, voltage, gas flow rate and temperature) and the output weld bead penetration.

2. MATERIALS AND METHOD

Mild steel plate of 10 mm thickness was cut into a dimension of 120x30 mm (length x width) each as shown in Figure 1. Sand paper was used to smoothen each of the two specimen to eliminate all possible coatings, corrosion or rust that may have accumulated on the material. The two steel plates were chamfered at 30°, after which, fusion welding was used to join the two plates together to form an angle of 60° with 2mm depth. The milling of the angle was done using a vertical milling machine. The welding was carried out with the plates properly clamped to avoid misalignment during welding process. Prior to welding, surface of the samples to be welded were cleaned using acetone in order to eliminate surface contamination, and welding was applied to fuse the two flat plates together. The weld bead penetration values

were measured using digital planimeter with 1-μm accuracy. K-type thermocouples were attached to the surface of the workpiece and the temperature was recorded at 20 points as the arc passed along the workpiece. Also, the welding torch passed over the plate at a height of 2.5mm from the workpiece at constant velocity of 1.72 mm/s. Design Expert 7.01 was used to deduce design of experiment for the welding parameters for 20 runs with, variable voltages ranging from 16-25V, variable currents ranging from 96-213A and variable gas flow rates ranging from 11-19 L/min respectively. Materials and specifications used for the welding experimentation are presented in Table 1.

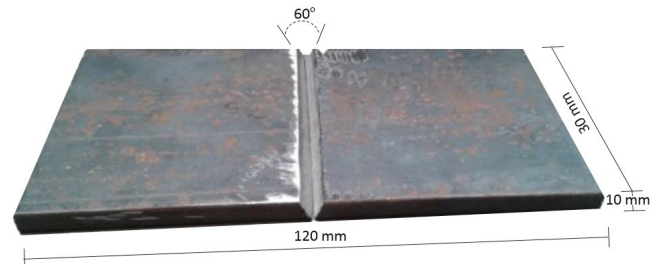


Figure 1. V-butt specimen of AISI 1020 Low Carbon Steel Plate

Table 1. Materials and Specifications used for the Welding Experimentation

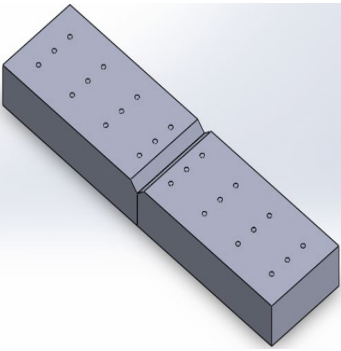
S/N	Material Specification	Welding Specification
1	Welding Type	Tungsten Inert Gas (TIG)
2	Material	AISI 1020 Low Carbon Steel Plate
7	Material Thickness	10 mm
8	Filler Material	ER 70 S-6
9	Joint Type	Butt Joint (V-groove)
10	Joint Preparation	Abrasive Clean (Sand paper)/Acetone Wipe
11	Joint Gap	2 mm
12	Welding Current	D.C.E.N (Direct Current Electrode Negative)
13	Pulse Width	0.8 Seconds
14	Filler Rod Angle	15°
15	Welding Torch Angle	45°
16	Fixed Frequency	60Hz
17	Torch Type	Pro-torch (TIG Torch)
18	Tungsten Type	2% thoriated
19	Tungsten Size	3/1326" Diameter x 25.4 mm
20	Torch Gas	Argon (100%)
21	Heat Input Ratio	10.75 KJ/min
22	Weight of Filler Rod	78.5 Kg/m ²
23	Welding machine	Dynasty 210 DX
24	Clamp type	G-clamp for clamping the work pieces
25	Vertical milling machine	For milling the V-groove angle

During welding the governing partial differential equation for 3D transient heat conduction is given by the thermal equilibrium relationship in equation 1;

$$\rho C_p \frac{\partial T}{\partial t} (x, y, z, t) = -\nabla \cdot q (x, y, z, t) + Q (x, y, z, t) \quad (1)$$

Where Q is the heat input, C_p is the specific heat, T is the temperature, ρ is density, q is the rate of heat flux, a, b, c , and t are the arc dimensions.

Table 2. Material Properties for 10 mm FE Model and Mesh Type

Material: AISI 1020	Properties	Finite Element Model	Solid Mesh
Model type	Linear Elastic Isotropic		
Failure criterion	Max von Mises Stress		
Yield strength	351.571 N/mm ²		
Tensile strength	420.507 N/mm ²		
Elastic modulus	200000 N/mm ²		
Poisson's ratio	0.29		
Mass density	7900 g/cm ³		
Shear modulus	77000 N/mm ²		
Melting Point	1738 K		

Given by equation 2, equivalent heat input for simulating the arc heating effects during TIG welding process can be deduced as the integration of both surface and body heat flux;

$$Q = Q_s + Q_b = \eta EI \tag{2}$$

Where, Q_s and Q_b denotes the heat input due to surface flux and body flux, η is the arc efficiency, E is the arc voltage and I is current.

Given equation 3 and 4, by the surface flux (Q_s) and body flux (Q_b) are usually expressed in the form of Gaussian distribution;

$$Q_s = \frac{3Q_s}{\pi ac} \exp\left(-\frac{3x^2}{a^2} - \frac{3z^2}{c^2}\right) \tag{3}$$

$$Q_b = \frac{6\sqrt{3}Q_b}{abc\pi\sqrt{\pi}} \exp\left(-\frac{3x^2}{a^2} - \frac{3y^2}{b^2} - \frac{3z^2}{c^2}\right) \tag{4}$$

The thermal reaction resulting from solid-to-liquid phase transformation can be due to increase in specific heat (C_p) input in the temperature between solidus and liquidus temperature range. In the welding process, latent heat of fusion is released in the phase transformation, thus, causing increase in the enthalpy (h) [15] given by equation 5;

$$h = \rho C_p T + \rho L_f f \rho C_p' T \tag{5}$$

Where, the latent heat of fusion is denoted by L_f , ρ is the density, f is the mass proportion of molten metal in the weldment, and C_p' is the increased specific heat. In the welding process, ρ is assumed as constant and f is given by equation 6 [16];

$$f = \begin{cases} 0 & T < T_s \\ \frac{T - T_s}{T_L - T_s} & T_s \leq T \leq T_L \\ 1 & T > T_L \end{cases} \tag{6}$$

When the temperature ranges from solidus to liquidus temperature, the equivalent specific heat C_p is deduced from equation 7;

$$C_p' = C_p + \frac{L}{T} \frac{T - T_s}{T_L - T_s} \tag{7}$$

Also, if temperature of the weld pool is above the melting point (T_m), the latent heat of evaporation (L_e) can be considered in the FE model by using the equivalent specific heat C_p'' given by equation 8;

$$C_p'' = C_p' + \frac{L_e}{T} \frac{T - T_b}{T_m - T_b} \tag{8}$$

For the FEM, the standard AISI 1020 was used for the modelling the low carbon steel plate, considering the temperature dependent properties of the FE model as shown in Table 2. However, mesh control was applied to the heat source, while curvature based mesh was used due to the ellipsoidal shape of the heat source. The model information is presented in Table 3.

Table 3. AISI 1020 Plate Model Information

Model Information for 10 mm Flat Plate			
Study name	TIG welding	Mesher Used	Curvature based mesh
Analysis type	Thermal (Transient)	Jacobian points	4 Points
Mesh type	Solid Mesh	Maximum element size	3.4556 mm
Solver type	FFEPlus	Minimum element size	0.69112 mm
Solution type	Transient	Total Nodes	218728
Total time	20 Seconds	Total Elements	154350

3. RESULTS AND DISCUSSION

The simulation was run for 20 runs using the design of experiment (Centre Composite Design Method). As presented in Figures 2, 4, 6, 8, 10, 12, 14 and 16, the temperature on the finite element welding profile represent the thermal distribution across the welded metal. Microstructure of the mild steel plate used in this study having undergone heating as a result of the welding process naturally set the electrons (within the metal lattice) into motion from a region of higher temperature to a region of lower temperature. However, with constant application of welding heat, a point is attained when melting temperature of the material is reach and the material begins to melt. The temperature values presented in Table 4 is the average temperature recorded over the nine (9) thermocouples attached to the surface of the material (for both Experimental and FEM approach), and represent the average temperature across the welded metal, while Figure 18 represents the regression plot for both methods The Experimental and FEM predicted weld bead penetration is also presented in Table 4.

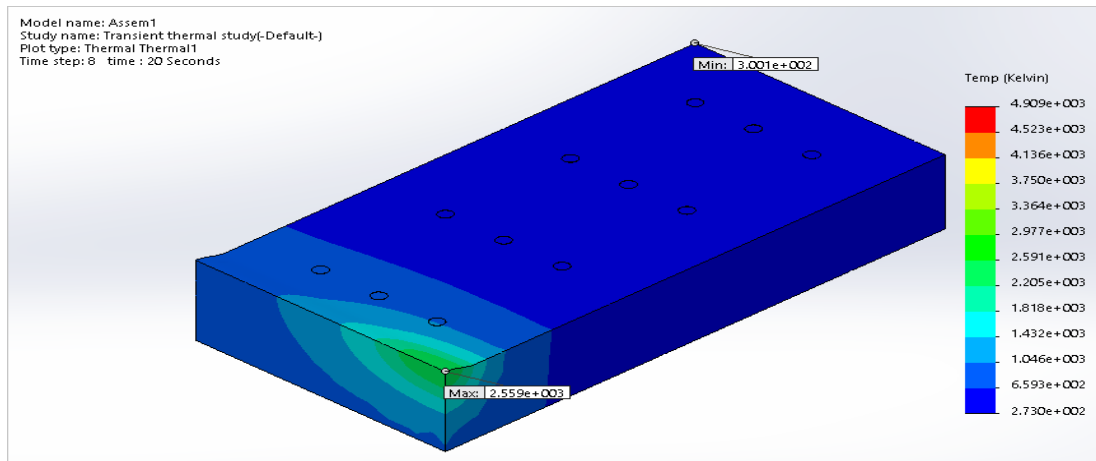


Figure 2. FEM Weld Bead Penetration Profile @ 96.14 amp, 22V and 15.50 L/min

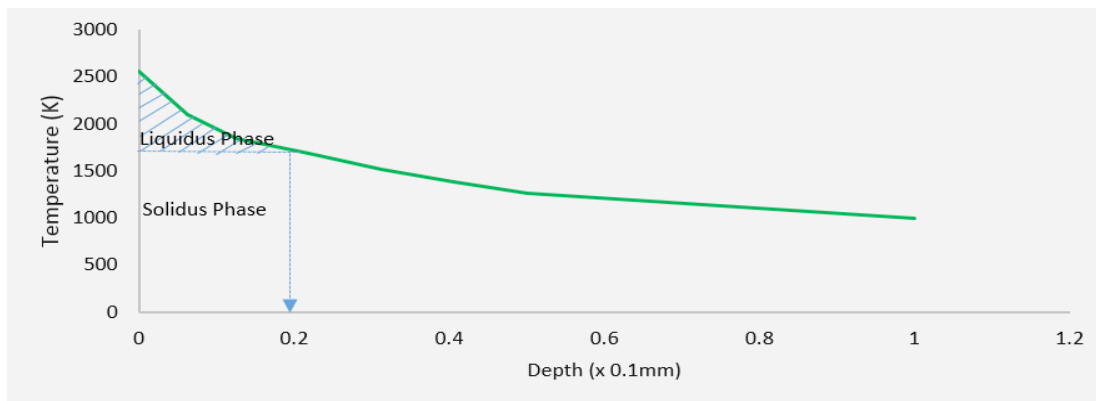


Figure 3. Plot of Temperature Vs Bead Depth @ 96.14 amp, 22V and 15.50 L/min

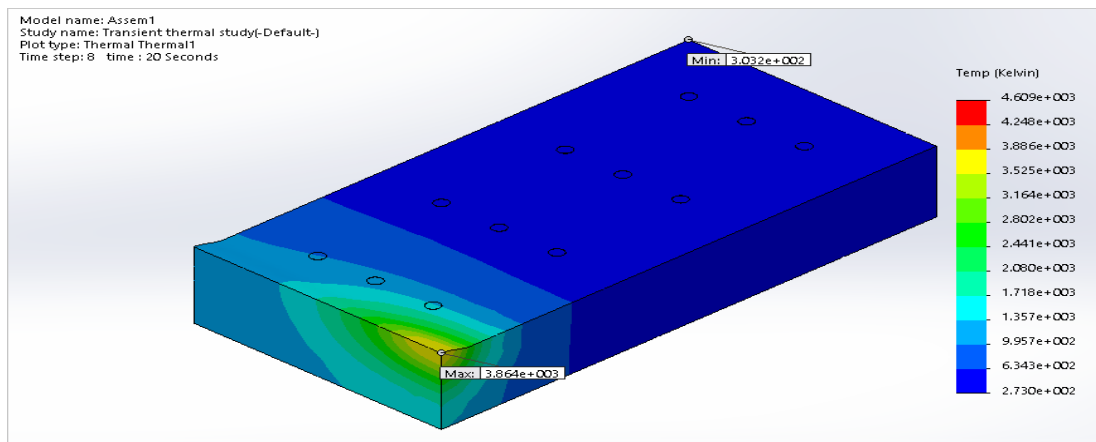


Figure 4. FEM Weld Bead Penetration Profile @ 190 amp, 19 V and 13 L/min

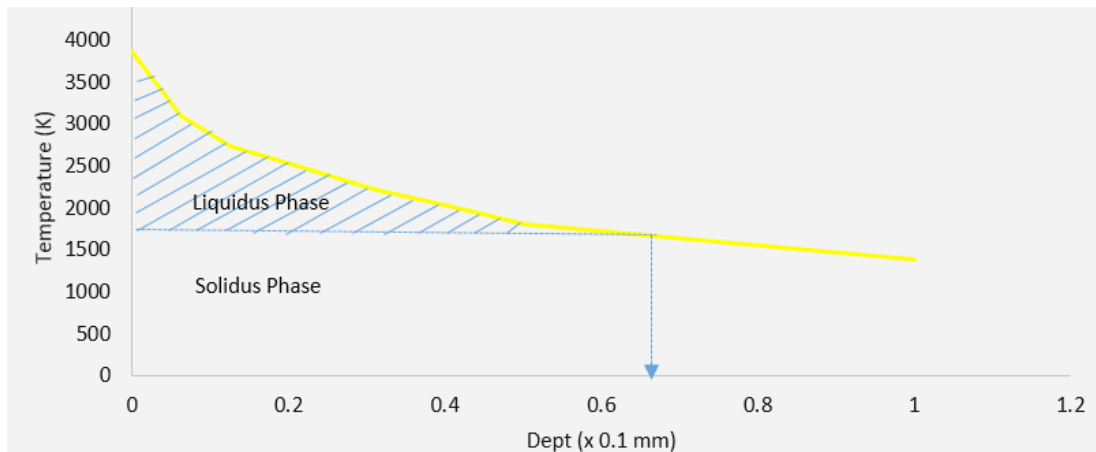


Figure 5. Plot of Temperature Vs Bead Depth @ 190 amp, 19 V and 13 L/min

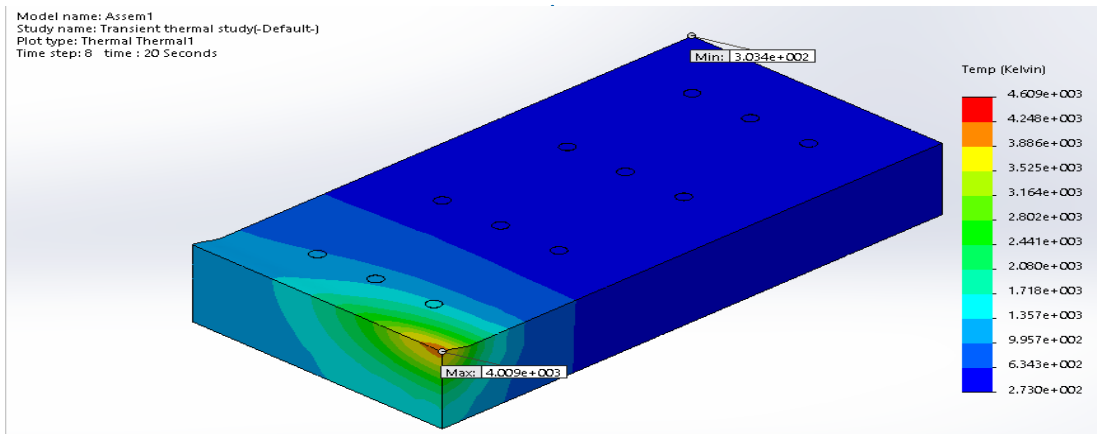


Figure 6. FEM Weld Bead Penetration Profile @ 155 amp, 22V and 15.50 L/min

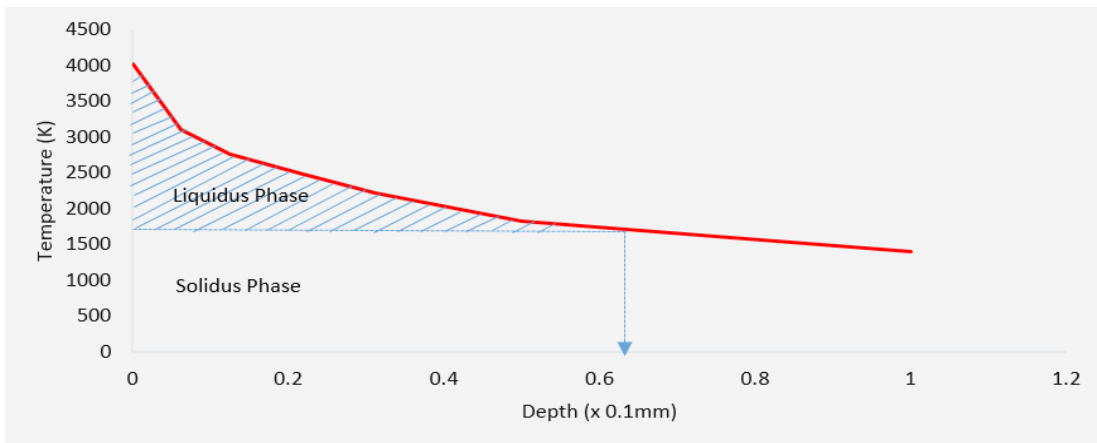


Figure 7. Plot of Temperature Vs Bead Depth @ 155 amp, 22V and 15.50 L/min

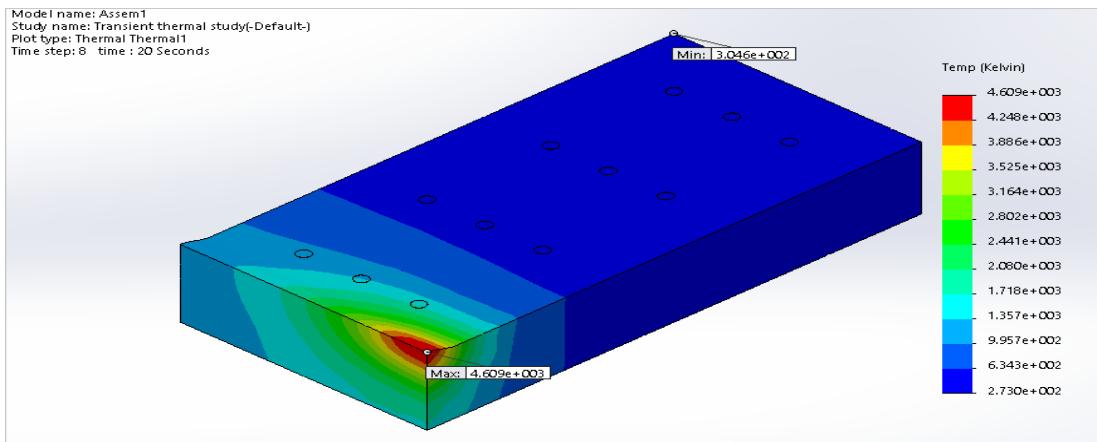


Figure 8. FEM Weld Bead Penetration Profile @ 190 amp, 19 V and 18 L/min

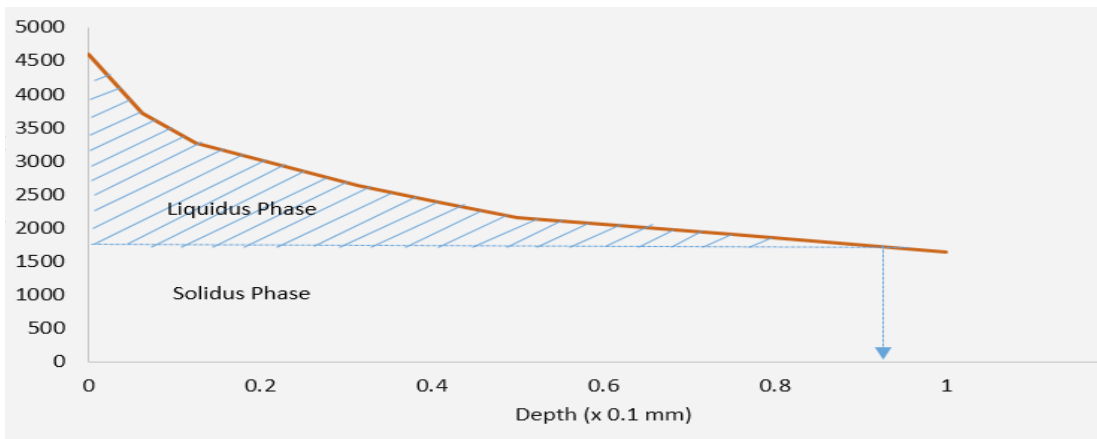


Figure 9. Plot of Temperature Vs Bead Depth @ 190 amp, 19 V and 18 L/min

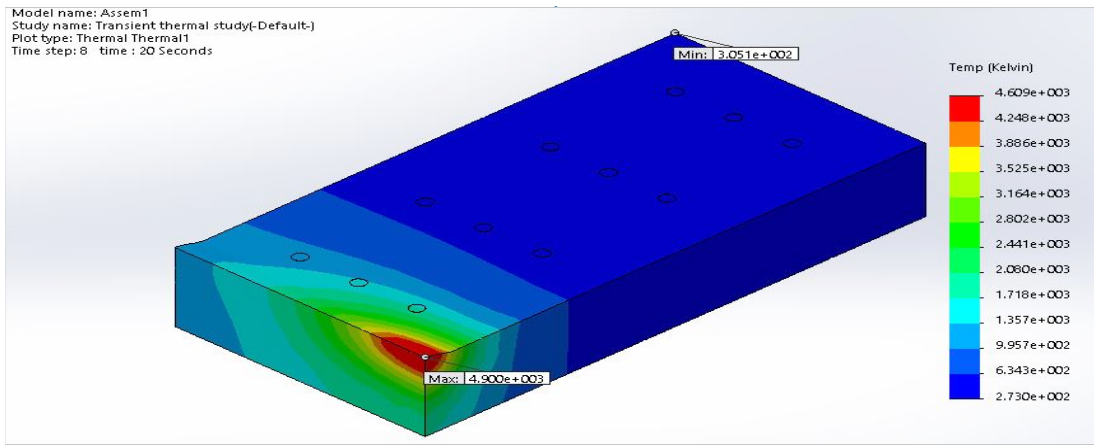


Figure 10. FEM Weld Bead Penetration Profile @ 155 amp, 27 V and 15.50 L/min

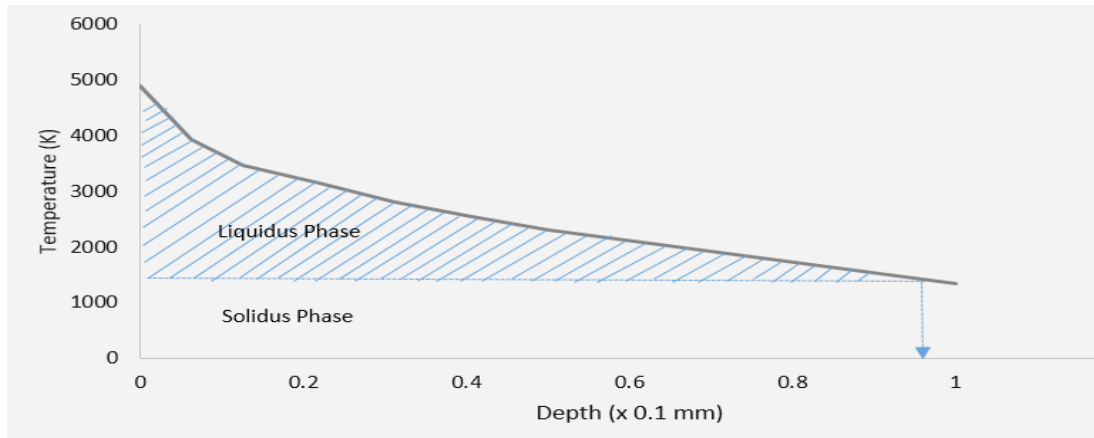


Figure 11. Plot of Temperature Vs Bead Depth @ 155 amp, 27 V and 15.50 L/min

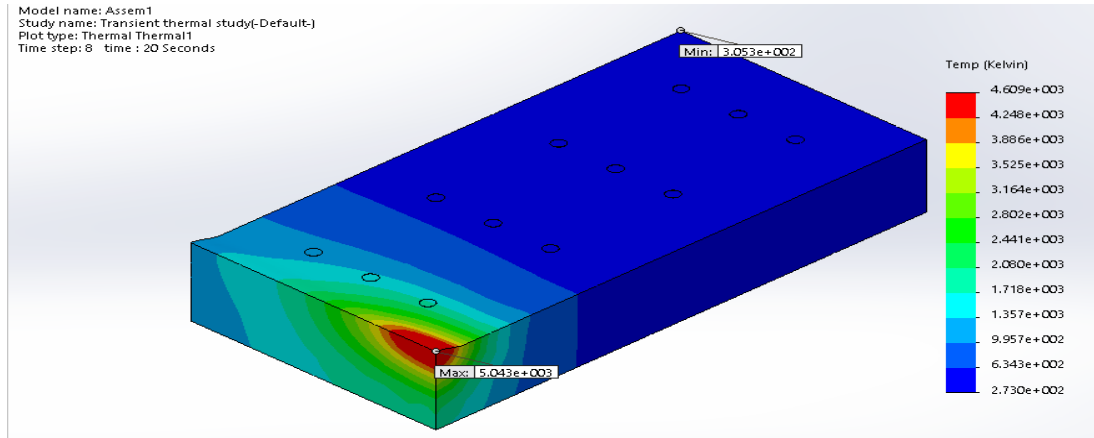


Figure 12. FEM Weld Bead Penetration Profile @ 190 amp, 25 V and 13 L/min

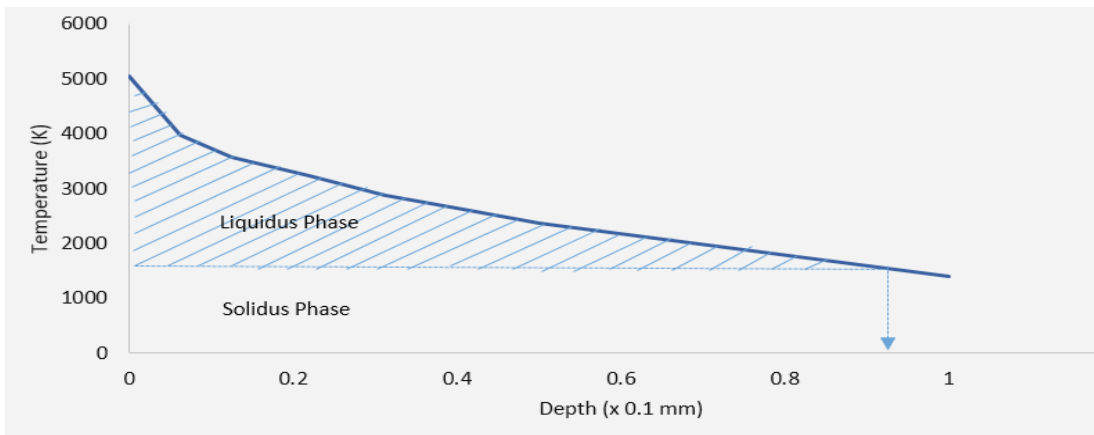


Figure 13. Plot of Temperature Vs Bead Depth @ 190 amp, 25 V and 13 L/min

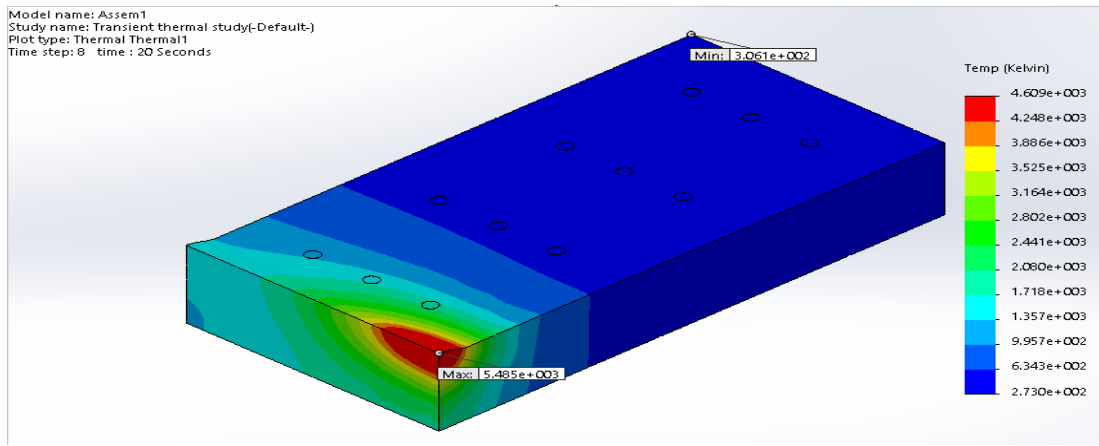


Figure 14. FEM Weld Bead Penetration Profile@ 213.86 amp, 22 V and 15.50 L/min

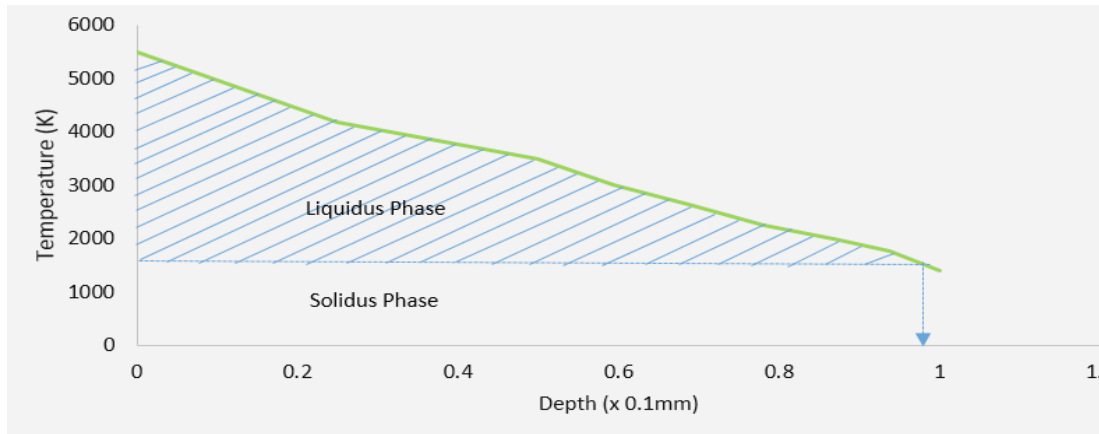


Figure 15. Plot of Temperature Vs Bead Depth @ 213.86 amp, 22 V and 15.50 L/min

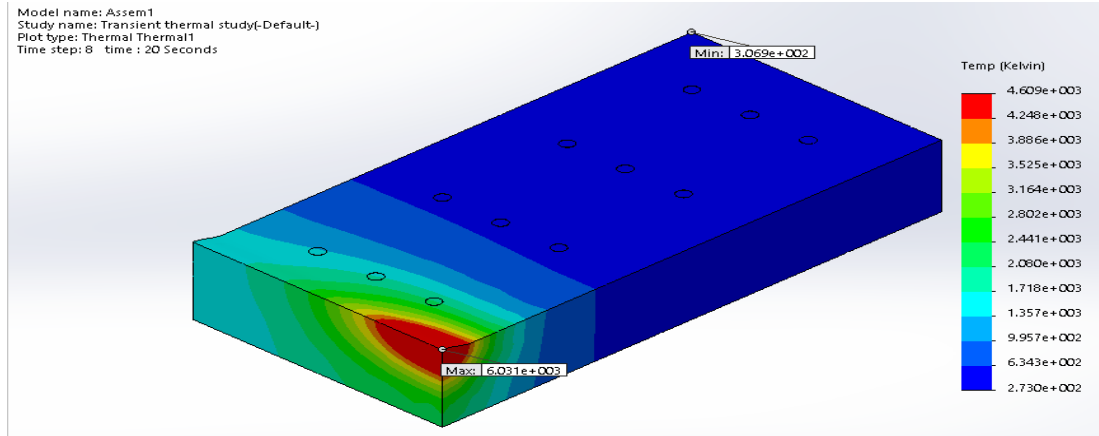


Figure 16. FEM Weld Bead Penetration Profile @ 190 amp, 25V and 18 L/min

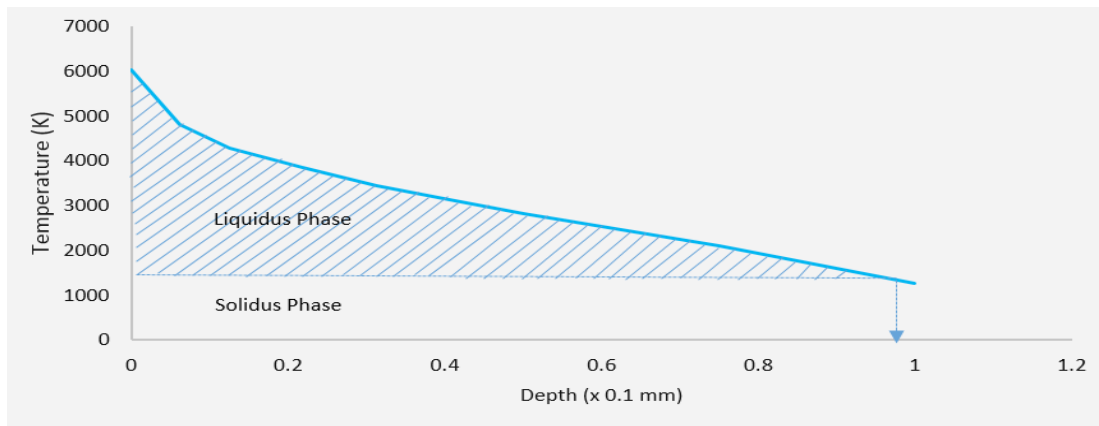


Figure 17. Plot of Temperature Vs Bead Depth @ 190 amp, 25V and 18 L/min

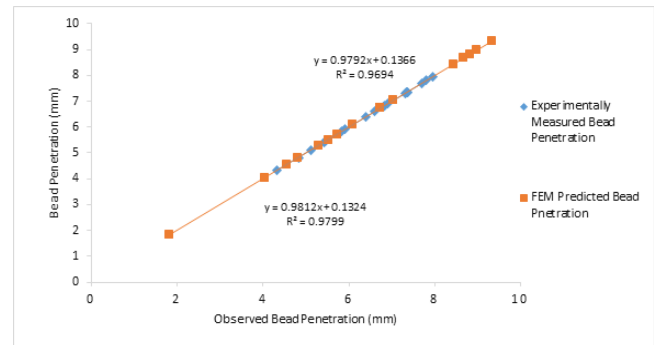
Table 4. Experimental and FEM Predicted Weld Bead Penetration

Weld Runs	Current (A)	Voltage (V)	Gas Flow Rate (L/min)	Temperature Distribution (°C)	Experimental Bead Penetration (mm)	FEM Bead Penetration (mm)
1	155.00	22.00	15.50	278.46	7.942	6.72
2	155.00	22.00	15.50	278.46	7.334	6.72
3	155.00	22.00	15.50	278.46	7.351	6.72
4	155.00	22.00	15.50	278.46	7.362	6.72
5	155.00	22.00	15.50	278.46	7.343	6.72
6	155.00	22.00	15.50	278.46	7.304	6.72
7	155.00	27.05	15.50	370.13	5.416	8.66
8	96.14	22.00	15.50	240.742	6.378	1.81
9	155.00	22.00	11.30	290.104	5.906	4.81
10	155.00	16.95	15.50	512.618	5.100	5.29
11	213.86	22.00	15.50	426.288	6.605	8.97
12	155.00	22.00	19.70	275.112	7.803	7.02
13	120.00	19.00	18.00	360.218	7.698	6.09
14	190.00	19.00	13.00	471.247	5.454	5.51
15	190.00	25.00	13.00	359.245	6.823	8.82
16	120.00	25.00	18.00	563.779	6.902	5.72
17	190.00	25.00	18.00	230.72	6.786	9.32
18	120.00	19.00	13.00	300.817	5.815	4.55
19	120.00	25.00	13.00	430.535	4.321	4.04
20	190.00	19.00	18.00	298.44	4.823	8.44

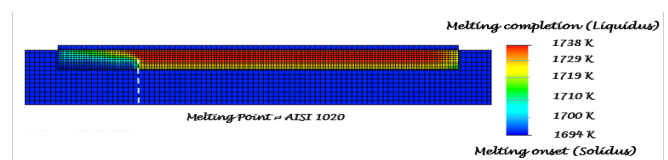
While current and gas flow rate are kept constant, increasing the voltage can result at increased bead penetration depth. This was observed in the 17th and 20th weld runs shown in Table 4, where constant current of 190.00 A, constant gas flow rate of 18.00 L/min and constant voltage of 25.00 V produced bead penetration of 6.786 mm for the welding experimentation and 9.32 mm for the FEM simulation, whereas, maintaining the same constant input variable for current (190.00 A) and gas flow rate (18.00 L/min) with varied voltage input of 19.00 V produced bead penetration of 4.823 mm for the welding experimentation and 8.44 mm bead penetration depth for the FEM simulation. Comparing the 17th and 20th weld runs for both experimental and FEM results, it is therefore observed that, increasing the welding voltage and maintaining the welding gas flow rate and welding current at constant rate can however deepen the depth of bead penetration in TIG welding applications. It was also observed in the first six (6) welding runs that maintaining a constant current of 155.00 A, a constant voltage of 22.00 V and a constant gas flow rate of 15.50 L/min produced the same value of bead penetration (6.72 mm) for weld runs 1-6 in the FEM simulation result whereas, slightly different bead penetration values (7.942 mm, 7.334 mm, 7.351 mm, 7.362 mm, 7.343 mm, 7.304 mm) where obtained for weld runs 1-6 in the welding experimentation. Variations in the bead penetration output results obtained from the welding experimentation may have been due to errors during the experimental setup, Calibration of the welding facilities, errors during measurement, error from the operator etc.

Comparing the finite element predicted bead penetration with the experimentally obtained weld bead penetration in Table 4, it was observed that bead penetration variation

from both approaches showed no wide disparity for the entire 20 welding runs carried out in this study. In other words, the coefficient of determination in the regression plot for both welding experimentation and FEM approach had close proximity (as shown in Figure 18), indication that the results obtained from both methods are close to being accurate.

**Figure 18.** Regression Plot for TIG Welding experimentation and FEM Prediction

Depending on the degree of response to applied heat, the atoms and electrons within the microstructure of the material continues to absorb heat until a point is reached where thermal equilibrium or saturation is attained and the material begins to melt. At thermal equilibrium, the atoms and electrons begin to move along its lattice until the material liquefies completely at critical temperatures. This thermal distribution is primarily a function of the material response to welding temperature and heat transfer in the material. The relationship between the material response to heat input and the welding bead penetration cannot be fully unravel without considering the solidus and liquidus temperature of the material which for the mild steel plate used in this study is presented in Figure 19.

**Figure 19.** Melting Profile for AISI 1020 Low Carbon Steel

The temperature at which solid metals begin to melt, but not completely melted is known as the solidus temperature while liquidus temperature quantifies the temperature at which a metal is completely melted. In addition, the metal is partly solid and partly liquid at temperatures between the solidus phase and liquidus phase whereas, the span of temperature from the point at which the metal begins to liquefy to the point at which the entire metal becomes molten liquid is known as melting range which for the mild steel plate used in this study was determined as 1694K-1738K as shown in Figure 19. However, below the solidus temperature phase, there was no phase transformation as the welded metal was continuously absorbing the heat applied from the welding but phase transformation occurred at the solidus temperature phase where the welded metal began to melt as a result of the welding heat. This can be observed in Figure 19 where the solidus temperature phase (1694 K) is identified as mel-

ting onset. Subsequent increase in temperature led to further transformation in the melting phase of the metal. This can be observed in the colour distribution in Figure 19, where the melting rate after solidus temperature was designated as light blue colour at a temperature of 1700 K, green colour at a temperature of 1710 K, yellow colour at a temperature of 1719 K, orange colour at a temperature of 1729 K and red colour at a melting temperature of 1738 K respectively. Dotted line on the melting profile in Figure 19 indicated the liquidus temperature phase, after which, the red colour continued, indicating a condition of complete melting where the metal at the weldment is entirely molten. For TIG welding process, the liquidus temperature phase is desired for deep penetration of weld bead, as rapid melting tends to occur at high temperature. This is further represented in Figures 2, 4, 6, 8, 10, 12, 14 and 16, which shows that high temperature is responsible for deep penetration of weld bead. This is because, the intense heat trapped within the weld pool tries to escape through any possible direction in the weldment and in the process spreads inwards and sideward in terms of depth and width. The inward direction of heat flow from the weld pool further react with the base metal where the molten metal settles to cause more penetration into the base metal until cooling and solidification occurs. From Figures 2, 4, 6, 8, 10, 12, 14 and 16, a range of colours known as Heat Affected Zones (HAZs) can be observed spreading outwards from the weld point and this indicate that part of the welded joint which has been heated to a temperature up to solidus of the parent material resulting in varying degree of influence on microstructure which depends upon a number of factors such as heating and cooling cycle, material composition, grain size (the smaller grain size, the higher the hardness) [17].

However as mentioned earlier, it is important to understand the melting morphology of a given metal before welding application as intense heat beyond the melting range and melting temperature of the metal may result in unwanted welding defects such as thermal cracking (crater crack, longitudinal crack, pear-shape crack etc), brittle fracture, high residual stress, undercut, distortions etc. Studies have revealed in recent times that joint penetration that is very shallow or less than the thickness of the weld joint may not have sufficient load carrying strength in service condition due to too narrow welding groove, too low welding amperage, too much arc length or arc voltage too fast or too slow electrode adjustment which could be salvage through the use of adequate welding amperage, arc length, arc voltage and the use of appropriate groove configuration [18]. However, Kamble and Rao [19] reported that intense distribution of heat around the weldment usually alters the chemical and mechanical properties of the material which depends upon the chemical composition of the bead and its geometry. The weld bead penetration depth in this study was scaled from 0-1 mm (parametric depth) in Solid Works which is the software that was used for the thermal analysis. To obtain the actual depth penetrated by the bead during welding, the

parametric depth was multiplied by 10. Thus, when reading the graphs presented in Figures 3, 5, 7, 11, 13, 15 and 17, the bead penetration was obtained by multiplying the depth traced at the melting temperature in the graphs by a factor of 10 to get the actual depth penetration in the 10 mm flat plate.

4. CONCLUSION

Finite element analysis was carried out using the commercial software package Solid Works 2017 version with thermal transient analysis to compare the weld bead penetration predicted from the model with experimentally determined bead penetration on mild steel plate of 10 mm thickness. By taking the averages between the values obtained by experimental method and the FEM, It was observed that the average temperature measured during the welding experimentation was 321°C with average penetration of 6.44 mm while the average FEM predicted temperature was 334°C with average FEM bead penetration of 6.48 mm. From the bead penetration values obtained experimentally and from FEM, there was proximity in the temperature distribution and corresponding weld bead penetration. From the regression plot, coherence was seen in the coefficient of determination R^2 (0.9799 and 0.9694) for both the FEM and experimentally determined bead penetration. This implies that both the FEM and experimental values generated similar responses to the welding parameters (current, voltage and gas flow rate), varied and exhibited constant trend, indicating that FEM is a better approach for validating the accuracy of welding experimental results. This is because, all simulations and iterations are performed by the software which calculates all the output variance according to the input variables unlike the experimental procedures which is prone to human error in terms of parametric adjustment, measuring, sample preparation etc. during the welding sequence.

REFERENCES

- [1] Razak, N. A., Shing, S. N. (2014). Investigation of effects of MIG welding on corrosion behaviour of AISI 1010 carbon steel. *Journal of Mechanical Engineering and Sciences* 7: 1168–78, Doi: 10.15282/jmes.7.2014.16.0114.
- [2] Nuraini, A. A., Zainal, A. S., Ariff, M. Hanim, A. (2014). The effects of Welding Parameters on Butt Joints Using Robotic Gas Metal Arc Welding. *Journal of Mechanical Engineering and Sciences*, 6: 988-994.
- [3] Singh, A. K., Dey, V., Rai, R. N. (2017). A Study to Enhance the Depth of Penetration in Grade P91 Steel Plate Using Alumina as Flux in FB TIG Welding. *Arab Journal of Science and Engineering*, 42: 4959-4970.
- [4] Memduh, K., Yukler, A., Bilici, M., Catalgol, Z. (2015). Effects Of Welding Current And Arc Voltage On Fcaw Weld Bead Geometry. *International Journal of Research in Engineering and Technology*, 4(9): 23-28.
- [5] Ikpe, A. E., Owunna, I., Ememobong, I. (2017). Effects of Arc Voltage and Welding Current on the Arc Length of Tungsten Inert Gas Welding (TIG). *International Journal of Engineering Technologies-IJET*, 3(4): 213-221.

- [6] Mohd, S., Mohd, P., Pratibha, K. (2013). Effect of MIG Welding Input Process Parameters on Weld Bead Geometry on HSLA Steel. *International Journal of Engineering Science and Technology*, Vol. 5(1): 200-212.
- [7] Bodude, M. A., Momohjimoh, I. (2015). Studies on Effects of Welding Parameters on the Mechanical Properties of Welded Low-Carbon Steel. *Journal of Minerals and Materials Characterization and Engineering*, 3: 142-153.
- [8] Sushant S. P. (2015). Theoretical and experimental study of MIG/MAG welding technique. *International Journal of Engineering Trends and Technology (IJETT)*, 24(3): 142-144.
- [9] Abbasi, K., Alam, S., Khan, M. I. (2012). An Experimental Study on the Effect of MIG Welding parameters on the Weld-Bead Shape Characteristics. *Engineering Science and Technology: An International Journal (ESTIJ)*, 2(4): 599- 602.
- [10] Satyaduttsinh P. C., Jayesh V., Tushar, M. (2014). A Review on Optimization of MIG Welding Parameters using Taguchi's DOE Method. *International Journal of Engineering and Management Research*, 4(1): 16-21.
- [11] Yadav, P. K., Abbas, M., Patel, S. (2014). Analysis of Heat Affected Zone of Mild Steel Specimen Developed due to MIG Welding. *International Journal of Mechanical Engineering and Robotic Research*, 3(3): 399-404.
- [12] Tewari, S. P., Gupta, A., Prakash, J. (2010). Effect of Welding Parameters on the Weldability of Material, *International Journal of Engineering Science and Technology*, 2(4): 512-516.
- [13] Ghazvinloo, H. R., Honarbakhsh-Raouf, A., Shadfar, N. (2010). Effect of arc voltage, welding current and welding speed on fatigue life, impact energy and bead penetration of AA6061 joints produced by robotic MIG welding. *Indian Journal of Science and Technology*, 3(2): 156-162.
- [14] Sudhakaran, R., Vel-Murugan, V., Sivasakthivel, P. S. (2012). Effect of Process Parameters on Depth of Penetration in Gas Tungsten Arc Welded (GTAW) 202 Grade Stainless Steel Plates Using Response Surface Methodology. *The Journal of Engineering Research*, 9(1): 64-79.
- [15] Cho, J. H., Na, S. J. (2009). Three-dimensional analysis of molten pool in GMA-laser hybrid welding. *Welding Journal*, 88: 35-43.
- [16] Piekarska, W., Kubiak, M. (2011). Three-dimensional model for numerical analysis of thermal phenomena in laser-arc hybrid welding process. *International Journal of Heat and Mass Transfer*, 54: 4966-4974.
- [17] Sura, N., Mittal, V. (2015). Experimental Study on Effects of Process Parameters on HAZ of Plain Carbon Steel Using GMAW. *International Journal of Latest Research in Science and Technology*, 4(2): 167-170.
- [18] www.kobelco.co.jp/english/welding/events/files/2015_KOBELCO_Defect.pdf, 2017.
- [19] Kamble, A. G., Rao, R. V. (2013). Experimental Investigation on the Effects of Process Parameters of GMAW and Transient Thermal Analysis of AISI321 Steel. *Advances in Manufacturing*, 1(4): 362-377.